Flow-response characteristics of the Kaijo Denki omni-directional sonic anemometer (TR-61B)

Mortensen, N.G.

Publication date:
1994

Document Version
Publisher's PDF, also known as Version of record

RISØ

Risø-R-704(EN)

Flow-Response Characteristics of the Kaijo Denki Omni-Directional Sonic Anemometer (TR-61B)

Niels G. Mortensen

Risø National Laboratory, Roskilde, Denmark
April 1994

Flow-Response Characteristics of the Kaijo Denki Omni-Directional Sonic Anemometer (TR-61B)

Risø-R-704(EN)

Niels G. Mortensen

Risø National Laboratory, Roskilde, Denmark
April 1994

Abstract This report describes a commercially available, three-dimensional sonic anemometer/thermometer, the Kaijo Denki DAT-300, fitted with an omni-directional sensor, the TR-61B probe head. Based on an analysis of the probe geometry and a comprehensive wind tunnel investigation it is found that the flow around the probe head is significantly distorted. Sonic-derived horizontal wind speed, wind direction and wind vector tilt deviate by as much as 15%, 5° and 3°, respectively, from the corresponding quantities in the wind tunnel. The flow distortion reflects strongly the geometry of the probe head and is partly dependent on the flow speed. Expressions are derived to assess the transducer shadow effect, but these alone cannot explain the response characteristics of the sonic. Instead, an ad-hoc calibration procedure is suggested, employing correction tables based on the wind tunnel measurements. The corrected horizontal and vertical wind speed components compare well to the wind tunnel, even though the vertical response shows some scatter. Preliminary field investigations support the correction scheme and suggest that the calibration may be stable over periods of several years.

Expressions for calculating the sound-virtual temperature from the transit times, taking into account the translation of the sound wave field due to the flow speed component perpendicular to the sound path, have been derived. An exact correction term to the sonic temperature output follows directly.

ISBN 87-550-1921-8
ISSN 0106-2840

Grafisk Service · Risø · 1994

Contents

1 Introduction

It has become increasingly important that studies in wind energy, diffusion, and air-sea interaction are supported by high-quality, remote measurements of atmospheric turbulence where such data must reliably accumulate over long periods. As a result, much emphasis has been placed on the development of durable fast-response meteorological instrumentation during recent years. In this report we describe a commercially available, omni-directional sonic anemometer/thermometer. Based on wind tunnel tests an extensive calibration procedure for the sonic is reported. Finally, field data collected over a two-year period from a horizontally homogeneous site in the western part of Denmark are described as both instrument validation and as an illustration of the utility of the sonic for providing long-term high-quality data.

2 The sonic anemometer/thermometer

The three-dimensional sonic system in question is a Kaijo Denki DAT-300 with an omni-directional sensor (TR-61B); see Fig. 1. The sensor consists of three pairs of acoustic transducers, each mounted in a streamlined casing with a length of 8 cm and a maximum diameter of 2 cm. The diameter of the transducer itself is 1.2 cm. The three intersecting paths are oriented at 120-degree azimuth intervals and inclined 45 degrees to the horizontal. The top and bottom of the array are connected by three struts with an elliptical cross-section (1.4×0.8 cm^2). The path length is 20 cm, giving a path length to transducer diameter ratio of ≥ 10.

Technical details of the measurement principles and operation of the instrument are given by Hanafusa et al. (1982) and Kaijo Denki (1982).

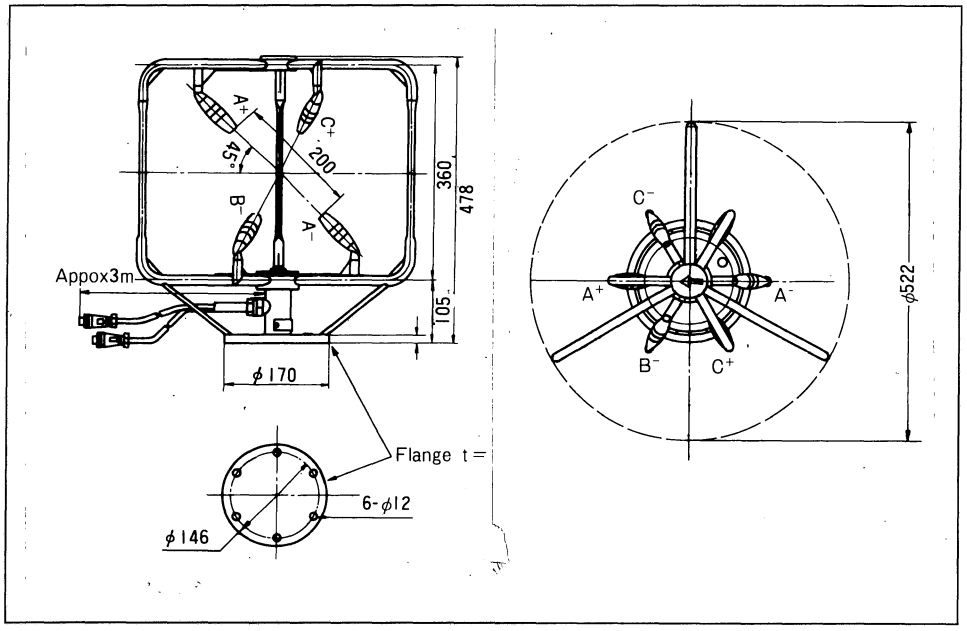

Figure 1. The Kaijo Denki TR-61B probe head (Kaijo Denki, 1982). Left and right in the figure correspond to north and south, respectively, when the probe is mounted in the atmosphere.

2.1 Principle of operation

Ultrasonic sound pulses are transmitted alternately in opposite directions between the two transducers, see Fig. 2.

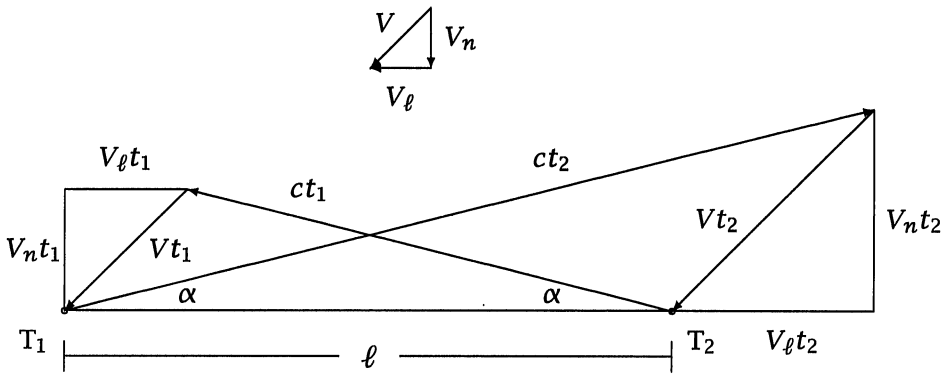

Figure 2. Sound ray diagram for one sonic path showing the principle of operation of the sonic anemometer. The transit times for sound pulses traveling from transducer T_1 *to* T_2 *and vice versa are* t_2 *and* t_1*, respectively.*

Assuming a uniform flow field the apparent speeds of the 'downwind' and 'upwind' traveling sound pulses are given by:

$$\frac{\ell}{t_1} = c \cdot \cos\alpha + S_\ell \quad \text{and} \quad \frac{\ell}{t_2} = c \cdot \cos\alpha - S_\ell \tag{1}$$

where ℓ is the distance between the two transducers, c is the speed of sound in (calm) air, S_ℓ is the flow speed along the sound path, and $\alpha = \arcsin(S_n/c)$; where S_n is the flow speed perpendicular to the sound path. The Kaijo Denki DAT-300 series measures the reciprocals of the transit times:

$$\frac{1}{t_1} = \frac{c \cdot \cos\alpha + S_\ell}{\ell} \quad \text{and} \quad \frac{1}{t_2} = \frac{c \cdot \cos\alpha - S_\ell}{\ell} \tag{2}$$

The difference between the reciprocals of the transit times is proportional to the flow speed along the acoustic path:

$$\frac{1}{t_1} - \frac{1}{t_2} = 2\frac{S_\ell}{\ell} \tag{3}$$

from which the following expression for flow speed S_ℓ is obtained:

$$S_\ell = \frac{\ell}{2}\left(\frac{1}{t_1} - \frac{1}{t_2}\right) \tag{4}$$

Given the path length, the wind speed can thus be determined by measuring the transit times only. This determination is in principle independent of atmospheric conditions, eg air temperature, humidity, and pressure.

2.2 Sonic coordinate systems

Zhang et al. (1986) derived the basic relations for the so-called UW sonic anemometer, the geometry of which is quite similar to that of the TR-61B probe. Their results in terms of the Kaijo Denki array and coordinate system are stated briefly below in (5)–(11).

In a right-handed, orthogonal coordinate system aligned with the array, the bottom triangle $A^-B^-C^-$ of transducers defines the horizontal x_1-x_2 plane, Fig. 3. The B^-C^- direction is taken as the x_1-axis and the x_2-axis is to the

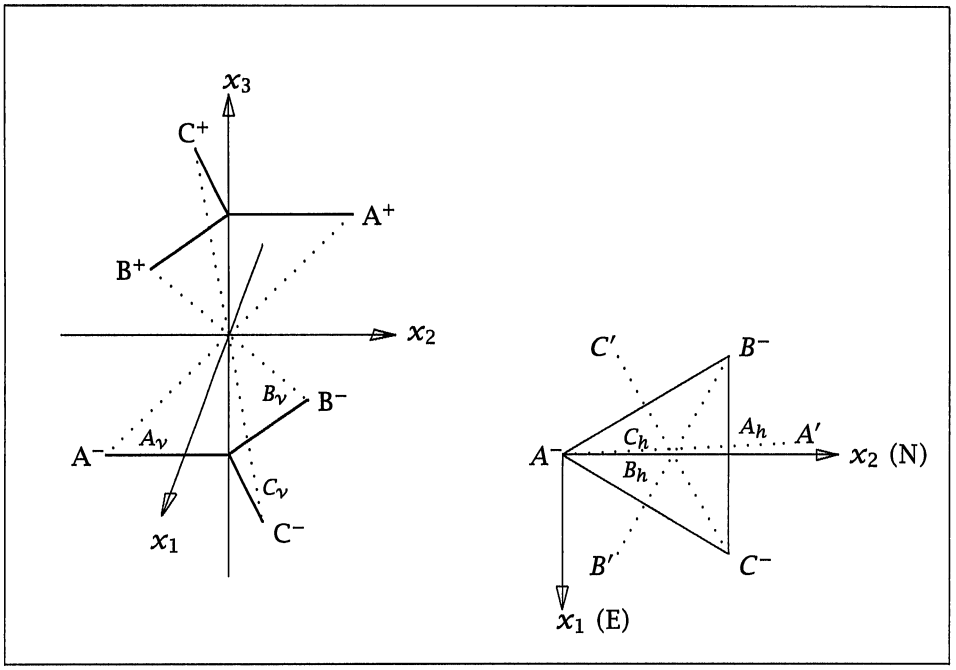

Figure 3. Geometry of the Kaijo Denki TR-61B probe head and associated coordinate systems (Kaijo Denki, 1982; Zhang et al, 1986).

left of and perpendicular to the x_1-axis. In this way the x_1- and x_2-axis correspond to east and north, respectively, when the anemometer is mounted in the atmosphere. The x_3-axis is perpendicular to the x_1-x_2 plane and upwards.

Let $\boldsymbol{t}_1$, $\boldsymbol{t}_2$, and $\boldsymbol{t}_3$ be three unit vectors along the sonic paths A^-A^+, B^-B^+, and C^-C^+, respectively. Then, from geometrical considerations:

$$\begin{aligned} \boldsymbol{t}_1 &= \sin A_h \cos A_v \boldsymbol{i}_1 + \cos A_h \cos A_v \boldsymbol{i}_2 + \sin A_v \boldsymbol{i}_3 \\ \boldsymbol{t}_2 &= \sin B_h \cos B_v \boldsymbol{i}_1 - \cos B_h \cos B_v \boldsymbol{i}_2 + \sin B_v \boldsymbol{i}_3 \\ \boldsymbol{t}_3 &= -\sin C_h \cos C_v \boldsymbol{i}_1 - \cos C_h \cos C_v \boldsymbol{i}_2 + \sin C_v \boldsymbol{i}_3 \end{aligned} \tag{5}$$

where $\boldsymbol{i}_1$, $\boldsymbol{i}_2$, and $\boldsymbol{i}_3$ are unit vectors along the x_1, x_2, and x_3 axes, respectively.

The wind vector can be expressed as the vector sum of its components along the x_1, x_2, and x_3 axes:

$$\boldsymbol{V} = U_1 \boldsymbol{i}_1 + U_2 \boldsymbol{i}_2 + U_3 \boldsymbol{i}_3 \tag{6}$$

The projections, S_i, of the same wind vector onto the three sonic paths are given by:

$$S_i = \boldsymbol{V} \cdot \boldsymbol{t}_i \qquad i = 1, 2, 3 \tag{7}$$

Using (5) and (6) we can write (7) as:

$$S_i = \sum_{j=1}^{3} a_{ij} U_j \qquad i = 1, 2, 3 \tag{8}$$

where the matrix $[a_{ij}]$ is given by:

$$[a_{ij}] = \begin{pmatrix} \sin A_h \cos A_v & \cos A_h \cos A_v & \sin A_v \\ \sin B_h \cos B_v & -\cos B_h \cos B_v & \sin B_v \\ -\sin C_h \cos C_v & -\cos C_h \cos C_v & \sin C_v \end{pmatrix} \tag{9}$$

Conversely, from (8) we can express the wind components U_i as:

$$U_i = \sum_{j=1}^{3} b_{ij} S_j \qquad i = 1, 2, 3 \tag{10}$$

where the wind components S_1, S_2, and S_3 along the three sonic paths are obtained from (4). The matrix $[b_{ij}]$ is the inverse of $[a_{ij}]$, so:

$$[b_{ij}] = [a_{ij}]^{-1} \qquad \text{and} \qquad \sum_k a_{ik}b_{kj} = \sum_k b_{ik}a_{kj} = \delta_{ij} \tag{11}$$

where δ_{ij} is the Kronecker delta. However, as pointed out by Zhang et al. (1986), $b_{ij} \neq a_{ji}$ because $\boldsymbol{t}_1$, $\boldsymbol{t}_2$, and $\boldsymbol{t}_3$ are not mutually perpendicular. For the simple case where the angles in Fig. 3 take their design values:

$$A_h = 0° \qquad B_h = C_h = 60° \qquad A_v = B_v = C_v = 45° \tag{12}$$

the $[a_{ij}]$ matrix and its inverse $[b_{ij}]$ reduce to:

$$[a_{ij}] = \begin{pmatrix} 0 & \frac{\sqrt{2}}{2} & \frac{\sqrt{2}}{2} \\ \frac{\sqrt{6}}{4} & -\frac{\sqrt{2}}{4} & \frac{\sqrt{2}}{2} \\ -\frac{\sqrt{6}}{4} & -\frac{\sqrt{2}}{4} & \frac{\sqrt{2}}{2} \end{pmatrix} \qquad [b_{ij}] = \begin{pmatrix} 0 & \frac{\sqrt{6}}{3} & -\frac{\sqrt{6}}{3} \\ \frac{2\sqrt{2}}{3} & -\frac{\sqrt{2}}{3} & -\frac{\sqrt{2}}{3} \\ \frac{\sqrt{2}}{3} & \frac{\sqrt{2}}{3} & \frac{\sqrt{2}}{3} \end{pmatrix} \tag{13}$$

From (10) and (13) the following expressions for the orthogonal wind speed components are then obtained:

$$\begin{aligned} U_1 &= \sqrt{\tfrac{2}{3}}(S_2 - S_3) \\ U_2 &= \tfrac{\sqrt{2}}{3}(2S_1 - S_2 - S_3) \\ U_3 &= \tfrac{\sqrt{2}}{3}(S_1 + S_2 + S_3) \end{aligned} \tag{14}$$

These are the expressions actually used in converting the along-path wind components to the corresponding orthogonal wind components (Kaijo Denki, 1982).

In practice, (13) and (14) hold only approximately because each individual probe head deviates slightly from the ideal design. Determination of the six characteristic angles of the probe gave the following values:

$$\begin{aligned} A_h &= 0.337° \qquad B_h = 59.899° \qquad C_h = 60.274° \\ A_v &= 45.107° \qquad B_v = 45.058° \qquad C_v = 45.288° \end{aligned} \tag{15}$$

The corresponding path lengths, measured from the surface of a 'dummy' transducer mounted in place of each of the transducers, are:

$$\ell_A = 21.379 \text{ cm} \qquad \ell_B = 21.346 \text{ cm} \qquad \ell_C = 21.379 \text{ cm} \tag{16}$$

Calculations using the design values (12) as well as the measured values (15) show only small differences.

2.3 Transducer shadow effect

One of the well-known errors in sonic anemometry is the transducer shadow effect, ie the underestimation of the wind components S_1, S_2, and S_3 due to velocity deficits in the wakes of the transducers along the acoustic paths (Kaimal, 1979). For a given flow speed the shadow effect is a function of the angle θ between the flow vector and the sonic path. Wyngaard and Zhang (1985) have suggested the following parameterization for Kaijo Denki type transducers:

$$\frac{S_i^{\mathrm{m}}}{S_i} = f(\theta_i) = 1 - (1 - C)\mathrm{e}^{-a \sin^2 \theta_i} \tag{17}$$

Here, S_i^{m} is the speed measured along path i and $S_i = V \cos \theta_i$ is the projection of the flow vector onto that path. The constants C and a are array-specific,

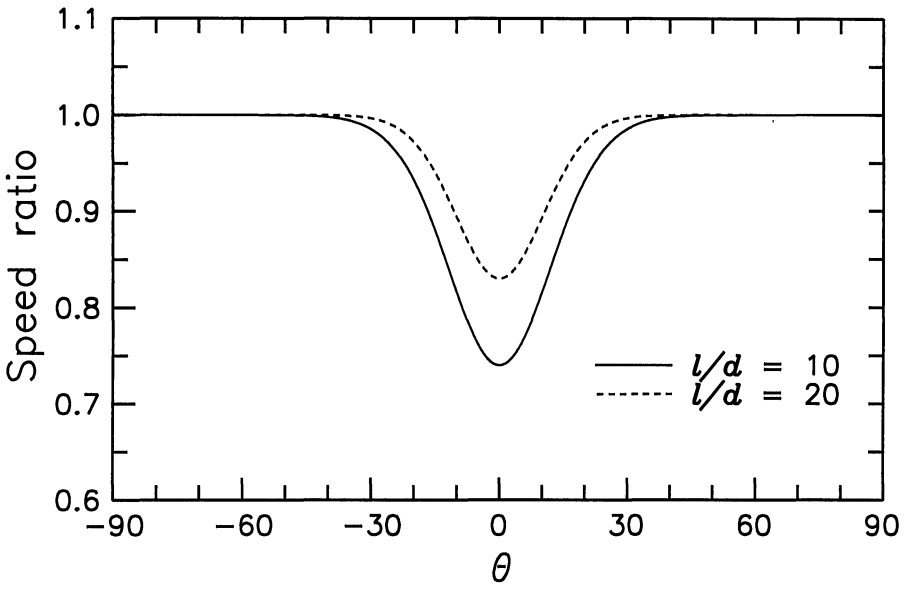

Figure 4. The attenuation of flow speed along a single sonic path (17) caused by the transducer shadow effect. Parameterization for Kaijo Denki type transducers according to Wyngaard and Zhang (1985).

ie correspond to a given ratio of ℓ/d, where ℓ is the distance between two transducers and d the diameter of the transducer, see Fig. 4.

From (6) we have:

$$\boldsymbol{V} = V\,[\cos\delta\cos\lambda\,\boldsymbol{i}_1 + \cos\delta\sin\lambda\,\boldsymbol{i}_2 + \sin\delta\,\boldsymbol{i}_3] \tag{18}$$

where λ is the wind vector azimuth angle in the (horizontal) x_1-x_2 plane and δ is the inclination of the wind vector $\boldsymbol{V}$ with respect to the same plane. The angles θ_i are then given by:

$$\cos\theta_i = \frac{1}{V}\,\boldsymbol{t}_i \cdot \boldsymbol{V} \qquad i = 1,2,3 \tag{19}$$

or, for the three sonic paths:

$$\begin{aligned}
\theta_1 &= \arccos[\cos A_v \cos\delta \sin(A_h + \lambda) + \sin A_v \sin\delta] \\
\theta_2 &= \arccos[\cos B_v \cos\delta \sin(B_h - \lambda) + \sin B_v \sin\delta] \\
\theta_3 &= \arccos[-\cos C_v \cos\delta \sin(C_h + \lambda) + \sin C_v \sin\delta]
\end{aligned} \tag{20}$$

The variation of θ_1, θ_2, and θ_3 with wind direction (ie with respect to N) is shown in Fig. 5.

Using (10), (17), and (8) we are now able to estimate the transducer shadow effect for different azimuth and inclination angles (Zhang et al, 1986):

$$\begin{aligned}
U_i^{\mathrm{m}} &= \sum_{j=1}^{3} b_{ij} S_j^{\mathrm{m}} \\
&= \sum_{j=1}^{3} b_{ij} f(\theta_j) S_j \\
&= \sum_{k=1}^{3}\sum_{j=1}^{3} f(\theta_j) b_{ij} a_{jk} U_k \qquad i = 1,2,3
\end{aligned} \tag{21}$$

Here $(U_1^{\mathrm{m}}, U_2^{\mathrm{m}}, U_3^{\mathrm{m}})$ are the measured components of the wind vector (U_1, U_2, U_3). As an example, in Fig. 6 the ratio of the measured to the actual horizontal wind component is shown for different inclination angles of the wind vector.

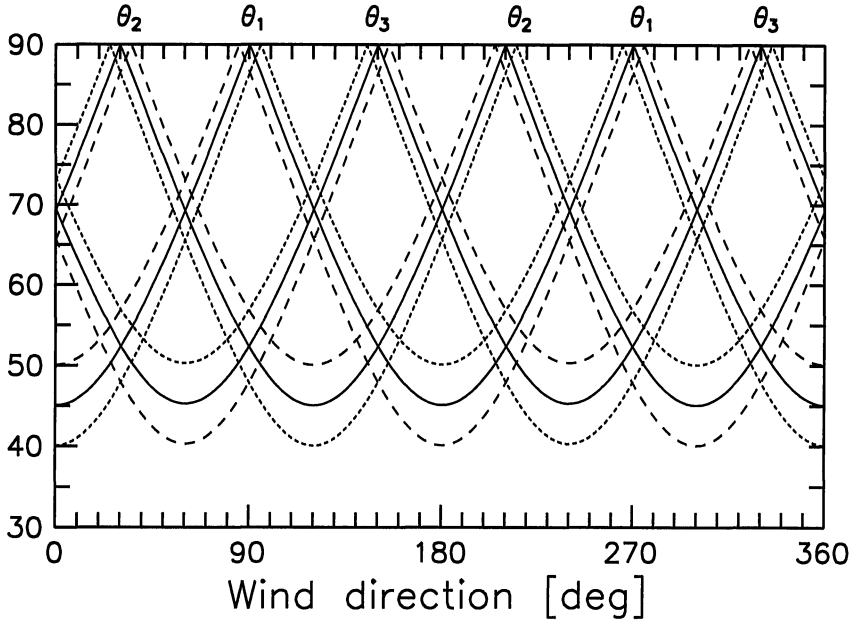

Figure 5. Variation of the angles θ_1, θ_2, and θ_3 between the wind vector and the three sonic paths with wind direction (20). Solid line: $\delta = 0°$, dashed line: $\delta = +5°$, dotted line: $\delta = -5°$.

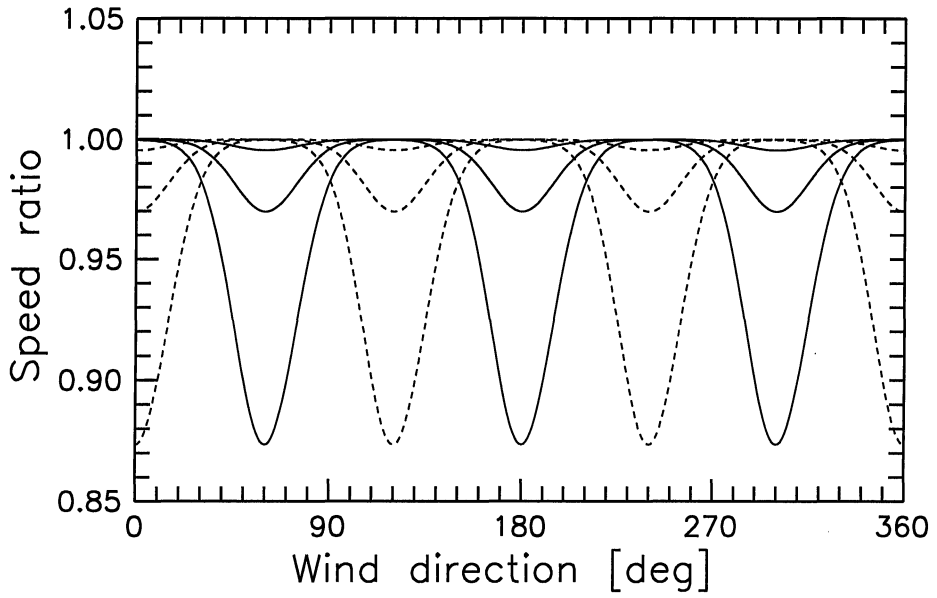

Figure 6. Attenuation of the horizontal wind component $\sqrt{U_1^2 + U_2^2}$ due to transducer shadow effects versus wind direction. Solid lines correspond to $\delta = +10°$, $+20°$, $+30°$, and dashed lines to $\delta = -10°$, $-20°$, $-30°$.

2.4 Mean-wind coordinates

As described above, the sonic anemometer provides measurements of the wind-vector components U_1, U_2, and U_3, obtained in a three-dimensional fixed Cartesian coordinate system, the x_1-axis of which conventionally points in the easterly, the x_2-axis in the northerly, and the x_3-axis in the vertical direction. The desired turbulence statistics, however, in terms of the covariance matrix

of the fluctuating velocity components u', v', w', are commonly referred to a Cartesian coordinate system, the x-axis of which is aligned in the mean wind direction whereas the mean cross- and vertical wind components are zero. We shall refer to this coordinate system as externally aligned.

To calculate the externally aligned quantities from the measurements in the fixed coordinate system, we first rotate the frame of reference around the x_3-axis of the probe head an angle $\lambda = \arctan(\overline{U}_2/\overline{U}_1)$, thereby aligning the x_1-axis with the mean wind direction in the x_1-x_2 plane of the probe head. In this turned coordinate system the mean wind speed becomes $(\overline{U}_1^2+\overline{U}_2^2)^{1/2}$, whereas the corresponding cross-wind component equals zero. Subsequently, we rotate around the x_2-axis an angle, δ, such that $\delta = \arctan(\overline{U}_3/(\overline{U}_1^2 + \overline{U}_2^2)^{1/2})$, thereby obtaining that also the mean vertical component in the realigned system becomes zero. The coordinate transformation reads:

$$\begin{pmatrix} u \\ v \\ w \end{pmatrix} = M \begin{pmatrix} U_1 \\ U_2 \\ U_3 \end{pmatrix} \tag{22}$$

Here $M = BA$, where B and A are unit matrices for right-handed coordinate rotation around the x_2- and x_3-axes, respectively:

$$M = \begin{pmatrix} \cos\delta\cos\lambda & \cos\delta\sin\lambda & \sin\delta \\ -\sin\lambda & \cos\lambda & 0 \\ -\sin\delta\cos\lambda & -\sin\delta\sin\lambda & \cos\delta \end{pmatrix} \tag{23}$$

Following these rotations, the covariance matrix C_a of the aligned wind components, u, v, w, relates to the covariance matrix C_f of the fixed-frame unaligned wind components, U_1, U_2, U_3, according to:

$$C_a = \begin{pmatrix} u' \\ v' \\ w' \end{pmatrix} (u', v', w') \tag{24}$$

$$= M \begin{pmatrix} U_1 \\ U_2 \\ U_3 \end{pmatrix} \left[M \begin{pmatrix} U_1 \\ U_2 \\ U_3 \end{pmatrix} \right]^{\mathrm{T}} \tag{25}$$

$$= M \begin{pmatrix} U_1 \\ U_2 \\ U_3 \end{pmatrix} (U_1, U_2, U_3)\, M^{\mathrm{T}} \tag{26}$$

$$= M C_f M^{\mathrm{T}} \tag{27}$$

2.5 Temperature measurement

Measuring air temperature with a sonic anemometer relies on the fact that the speed of sound in air, c, is dependent on the absolute temperature T: dc/dT is about 0.6 ms^{-1} per degree for dry air.

The sum of the reciprocals of the transit times in (2) is proportional to the speed of sound:

$$\frac{1}{t_1} + \frac{1}{t_2} = 2\frac{c \cdot \cos\alpha}{\ell} \tag{28}$$

Since $\cos^2\alpha = 1 - \sin^2\alpha = 1 - (S_n/c)^2$ we get the following (exact) expression for the speed of sound:

$$c^2 = \frac{\ell^2}{4}\left(\frac{1}{t_1} + \frac{1}{t_2}\right)^2 + S_n^2 \tag{29}$$

The speed of sound in moist air depends on the absolute temperature as well as the water vapor content through the virtual temperature, T_v:

$$c^2 = \gamma R_d T_v = \gamma R_d T\,(1 + 0.61q) \tag{30}$$

where $\gamma = c_p/c_v$ is the ratio of specific heats, R_d is the gas constant for dry air, T is the absolute temperature, and q is the specific humidity. The specific heats for moist air can be expressed as:

$$\begin{aligned} c_p &= qc_{pv} + (1-q)c_{pd} = c_{pd}(1 + 0.84q) \\ c_v &= qc_{vv} + (1-q)c_{vd} = c_{vd}(1 + 0.94q) \end{aligned} \tag{31}$$

where c_{pv} and c_{vv} are the specific heats for water vapor and c_{pd} and c_{vd} are the specific heats for dry air, respectively. Inserting in (30) and neglecting higher order terms:

$$c^2 = \gamma_d R_d T\,(1 + 0.51q) \qquad q \ll 1 \tag{32}$$

Here, $\gamma_d = c_{pd}/c_{vd}$ is the ratio of specific heats for dry air. The temperature $T(1 + 0.51q)$ is referred to as the sound virtual temperature, T_{sv}.

In order to determine directly the sound-virtual temperature the sonic temperature signal should be calculated (on-line or from the recorded time-series) as:

$$T_{sv} = \frac{\ell^2}{4\gamma_d R_d}\left(\frac{1}{t_1} + \frac{1}{t_2}\right)^2 + \frac{S_n^2}{\gamma_d R_d} \tag{33}$$

This follows from (29) and (32). For sonic probes with a vertical sound path, the wind speed normal to the temperature-measuring path, S_n, would be the horizontal wind speed, so $S_n^2 = (U_1^2 + U_2^2) = (u^2 + v^2)$. For the TR-61B probe, however, all three paths are inclined 45° to the vertical.

The temperature signal is apparently obtained from the A-path of the TR-61B probe (Kaijo Denki, 1982). The wind speed component along this path, S_1, can be found from (8) and (13):

$$S_1 = \tfrac{\sqrt{2}}{2}(U_2 + U_3) \tag{34}$$

Since the length of the wind vector, S, is given by $\sqrt{U_1^2 + U_2^2 + U_3^2}$, the wind component normal to the A-path is then:

$$S_n^2 = S^2 - S_1^2 = U_1^2 + \tfrac{1}{2}(U_2 - U_3)^2 \tag{35}$$

From (33) and (35) the sound virtual temperature can now be expressed as:

$$T_{sv} = \frac{\ell^2}{4\gamma_d R_d}\left(\frac{1}{t_1} + \frac{1}{t_2}\right)^2 + \frac{U_1^2 + \frac{1}{2}(U_2 - U_3)^2}{2\gamma_d R_d} \tag{36}$$

The temperature output signal provided by the Kaijo Denki DAT-300 is calculated using only the transit times t_1 and t_2 (Kaijo Denki, 1982), corresponding to the first term on the right-hand side of (36). The sonic temperature output, T_{KD}, and the sound virtual temperature thus differ by an amount given by:

$$T_{sv} - T_{KD} = \frac{S_n^2}{\gamma_d R_d} = \frac{U_1^2 + \frac{1}{2}(U_2 - U_3)^2}{2\gamma_d R_d} \tag{37}$$

The significance of this crosswind contamination on the temperature standard deviations and fluxes have recently been assessed by Kaimal and Gaynor (1991).

3 Sonic internal flow distortion

Because the sonic probe is designed to be stationary in the field with a varying wind vector, the distortion of the flow speed and direction (induced by the transducers and their supporting struts) was examined under controlled wind tunnel conditions. Calibration of the sonic was performed in the wind tunnel of the Danish Maritime Institute which has a cross-section of 2.76 m × 1.80 m ($w \times h$). Wind speeds of 3, 5, 7.5, 10, and 15 ms^{-1} were used and turbulence levels were artificially screened to low levels (< 1 %). The flow speed in the tunnel was measured with a pitot-static tube and a precision pressure transducer. The probe head was systematically rotated 360 degrees in the horizontal and through the range of +5 to −5 degrees in the vertical. The resolution in azimuth was 1 degree for horizontal flow at 10 ms^{-1}, 5 degrees for horizontal flow at other speeds, and 30 degrees for inclined flow.

3.1 Horizontal flow

The main characteristics of the flow deformation for horizontal, laminar conditions were investigated in detail at a flow speed of approx. 10 ms^{-1} by rotating the probe 360° in the horizontal in 1° steps. The results are depicted in Fig. 7 (a, b, c). It appears that the speed ratio (defined as the ratio of the sonic-measured wind speed to the true wind speed) is roughly 1.0 when averaged over azimuth, even though a systematic variation of one-degree factors on the order of 10% was observed. With reference also to Fig. 7, the supporting struts reduce the wind speed considerably, whereas the flow speeds up when directed unobstructed towards the transducers. The wind vector was found to be tilted upwards an average of about 1° for all azimuth directions; and both the tilt and horizontal deflection curves depend strongly on the geometry of the sensor.

A close look at Fig. 7 reveals that the horizontal response is not entirely 120°-symmetric as would be expected from the geometry of the probe. To investigate this further we present speed ratios versus azimuth angle for three different flow speeds in Fig. 8. It is apparent that the speed ratios show a significant dependency on wind speed. At the highest flow speed investigated the response is approximately 120°-symmetric, however at lower speeds the response becomes more and more asymmetric. This flow speed dependency can be described as a 360° modulation and is probably due to the mounting of the signal cables below the base of the sonic probe head, see Fig. 7. The cables are attached to a point at 0° (corresponding to due north), ie at right angles to the direction where the speed dependency has its maximum amplitude. The effect diminishes with increasing wind speed and becomes insignificant at speeds greater than $\approx$ 10 ms^{-1}.

In general, therefore, the speed ratio F is a function of both wind speed U and wind direction Θ:

$$\frac{U_s}{U_t} = F(U, \Theta) \tag{38}$$

where U_s is the sonic-derived wind speed and U_t is the true (tunnel) wind speed. If we assume that the velocity sensitivity disappears at wind speeds greater than $\approx$ 10 ms^{-1} ($F(10, \Theta) \approx F(\infty, \Theta)$) and that the dependency is a simple sinusoidal modulation we obtain the following simple expression for the variation of the speed ratio:

$$F(U, \Theta) = F(10, \Theta) + f(U, \Theta) = F(10, \Theta) + [a(U)\sin(\Theta + \phi) + b(U)] \tag{39}$$

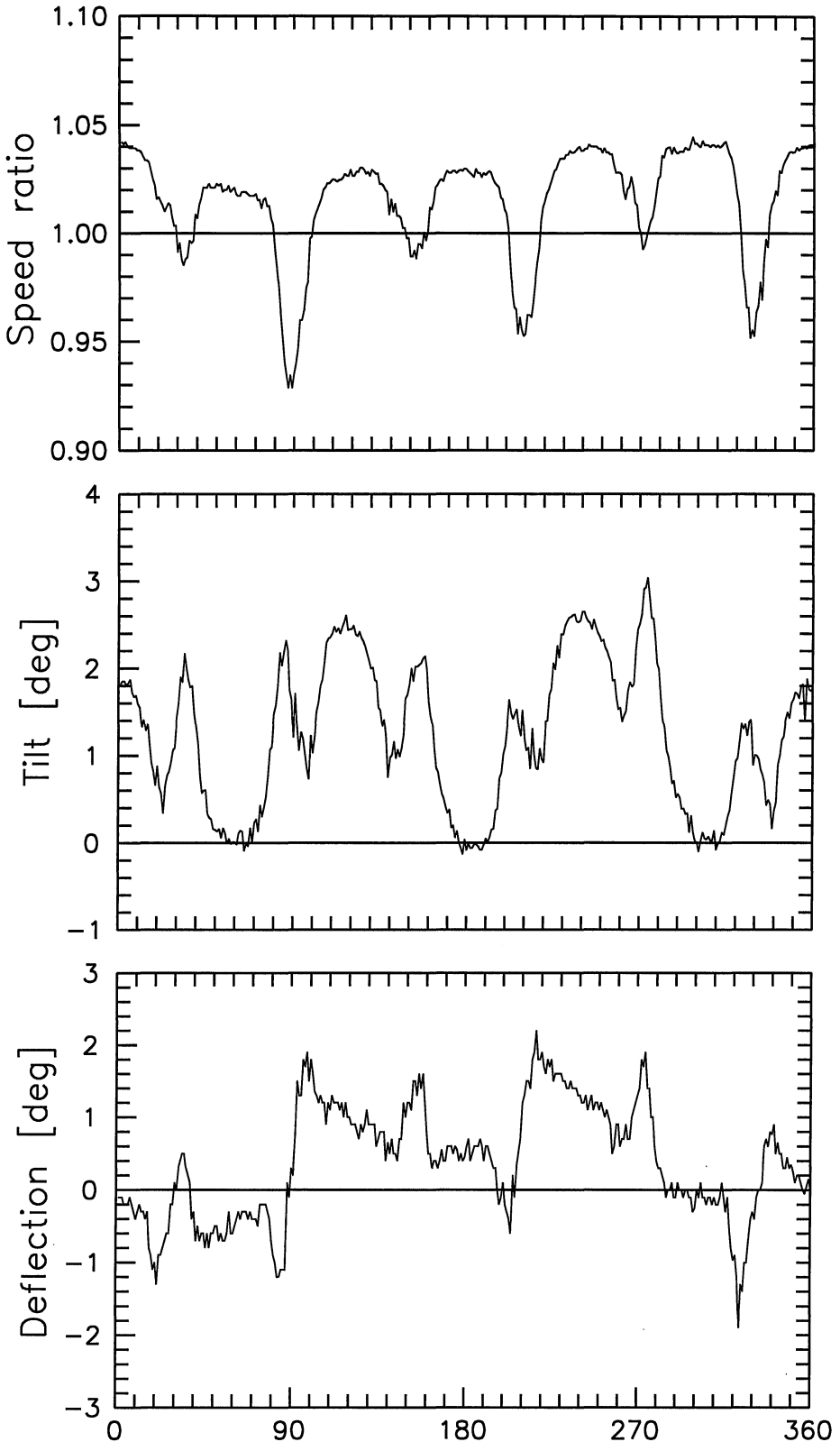

Figure 7. The sonic response to a laminar, horizontal flow of 10 ms^{-1} for different azimuth angles in a wind tunnel. The resolution in azimuth is 1°. *a) Speed ratio =* U_{sonic}/U_{true}. *b) Positive tilt* ($\alpha_s - \alpha_t > 0$) *indicates upward tilt of the wind vector. c) Positive deflection* ($\Theta_s - \Theta_t > 0$) *indicates clock-wise deflection of the wind vector.*

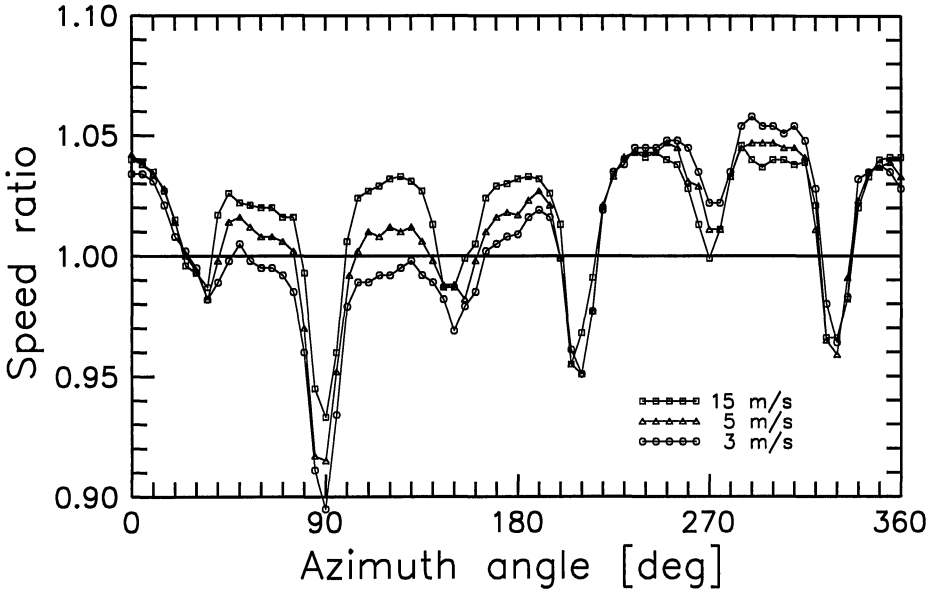

Figure 8. Sonic speed ratios versus azimuth angle for different flow speeds in a wind tunnel. The resolution in azimuth is 5°. For the sake of legibility only data at 3, 5, and 15 ms^{-1} are shown.

Here, $F(10,\Theta)$ is the measured variation of U_s/U_t (Fig. 7 a). The difference between the speed ratio at 10 ms^{-1} and speed ratios at 3, 5, and 15 ms^{-1} are shown in Fig. 9. It appears that a sinusoidal function describes the data quite well.

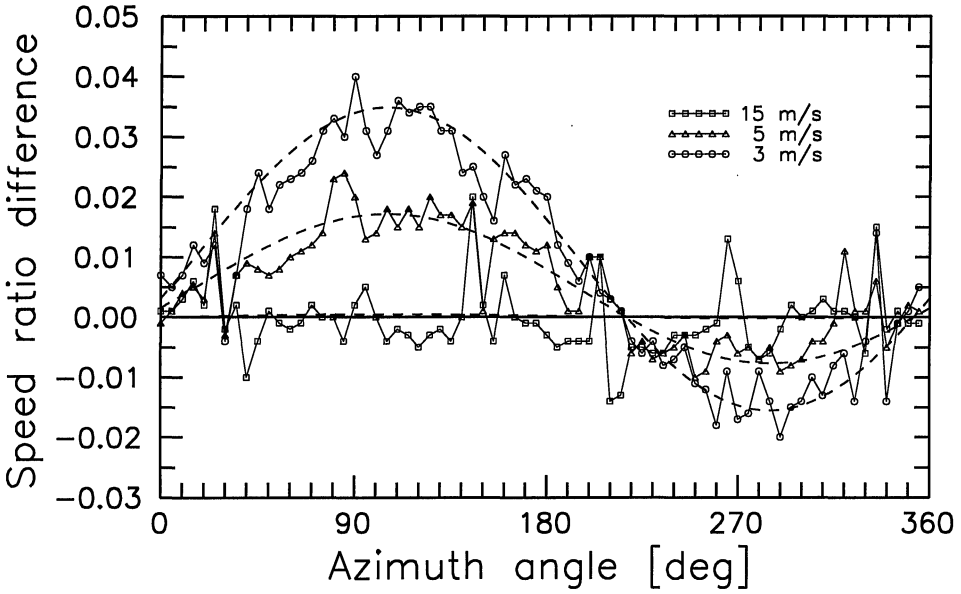

Figure 9. Speed ratio differences versus azimuth angle for three different flow speeds in a wind tunnel, see Fig. 8. Also shown are sinusoidal curves fitted to the measured data.

Wind direction

One may suspect that the origin of this velocity dependency in the speed ratios might also affect the deflection and tilt of the wind vector. In Fig. 10 the probe-induced deflection of the wind vector versus azimuth angle is shown for three different flow speeds. It is clear that the deflection is also dependent on the

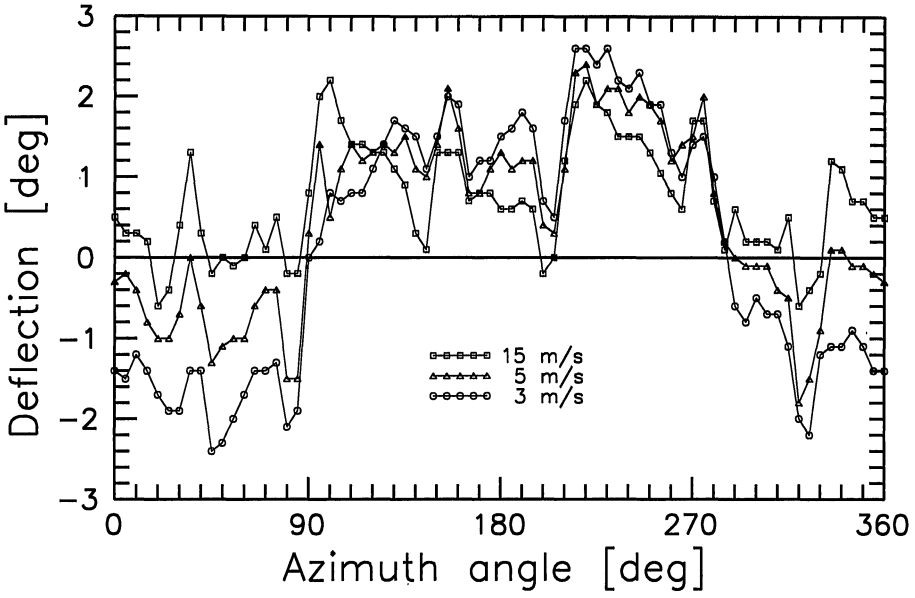

Figure 10. Deflection of the wind vector versus azimuth angle for three different flow speeds in a wind tunnel. The resolution in azimuth is 5°. For the sake of legibility only data at 3, 5, and 15 ms^{-1} are shown.

speed of the flow, ie $\Theta_s - \Theta_t = G(U,\Theta)$, where Θ_s is the sonic-derived wind direction and Θ_t is the direction obtained from the tunnel, ie the turntable on which the sonic is mounted. Note, that the maximum errors occur at a wind direction shifted approximately 90° compared to the speed ratio. This is qualitatively in accordance with the assumption that the signal cables are responsible for the speed-dependent flow distortion. Again, the effect can be described as a 360°-modulation and a simple sinusoidal function fits the data rather well, see Fig. 11. In this case we assume that the velocity sensitivity disappears at wind speeds greater than ≈ 15 ms^{-1} ($G(15,\Theta) \approx G(\infty,\Theta)$) and therefore obtain the following expression for the corresponding deflection function:

$$G(U,\Theta) = G(15,\Theta) + g(U,\Theta) = G(15,\Theta) + [a(U)\cos(\Theta+\phi) + b(U)] \quad (40)$$

Since the finest resolution in $G(U,\Theta)$ occurs at 10 ms^{-1} we note that $G(15,\Theta) = G(10,\Theta) - g(10,\Theta)$.

Tilt of wind vector

The probe-induced tilt of the wind vector for three different flow speeds is shown in Fig. 12. In contrast to the speed ratio and deflection, the tilt apparently shows no systematic variation with flow speed, other than a slight change in the mean tilt (ie averaged over azimuth): from $\overline{\alpha}$ at 15 ms^{-1} to $\overline{\alpha} + 0.3°$ at 3 ms^{-1}.

As described above the flow-speed dependent modulations of both the speed ratio and the deflection are modeled quite well by sine curves. The amplitude

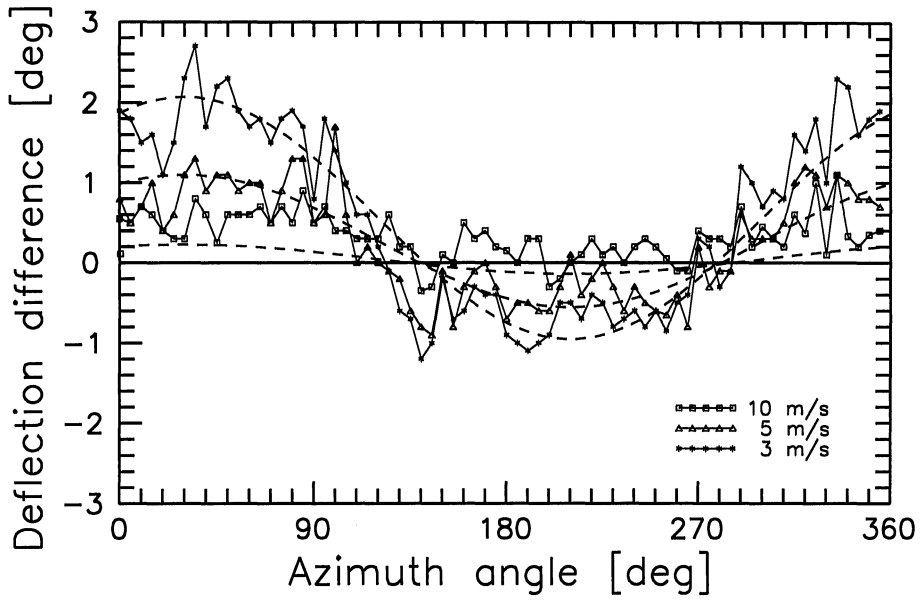

Figure 11. Wind vector deflection difference versus azimuth angle for three different flow speeds in a wind tunnel, see Fig. 10. Also shown are sinusoidal curves fitted to the measured data.

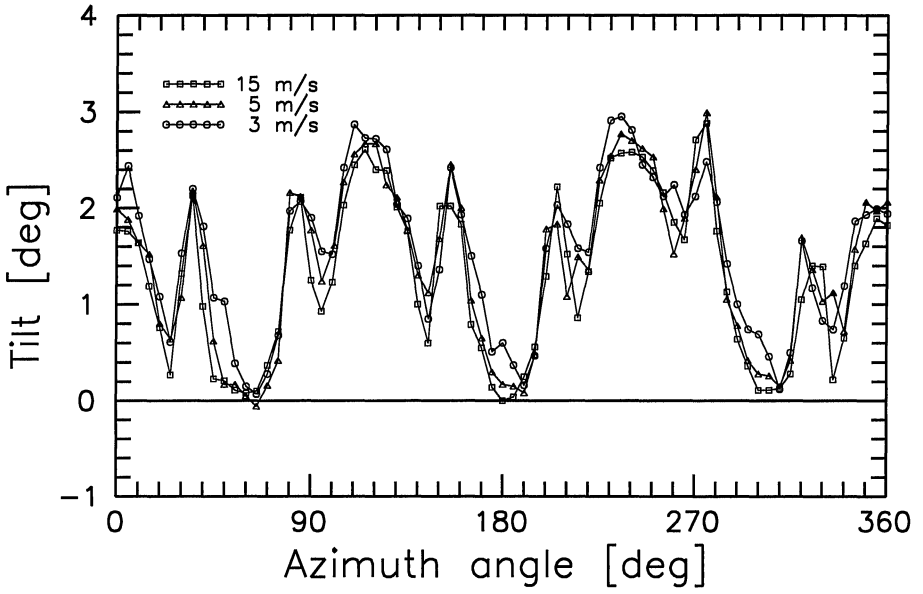

Figure 12. Tilt of the wind vector versus azimuth angle for three different flow speeds in a wind tunnel. The resolution in azimuth is 5°. For the sake of legibility only data at 3, 5, and 15 ms^{-1} are shown.

and bias of these functions, as well as the change in the mean tilt, are plotted versus flow speed in Fig. 13. The rather scarce data points are described well by exponential functions. Extrapolating these fits implies that the wind speed dependent errors in the sonic-measured wind speed, direction, and tilt may be substantial at very low wind speeds; approximately 10%, 5°, and 0.8°, respectively.

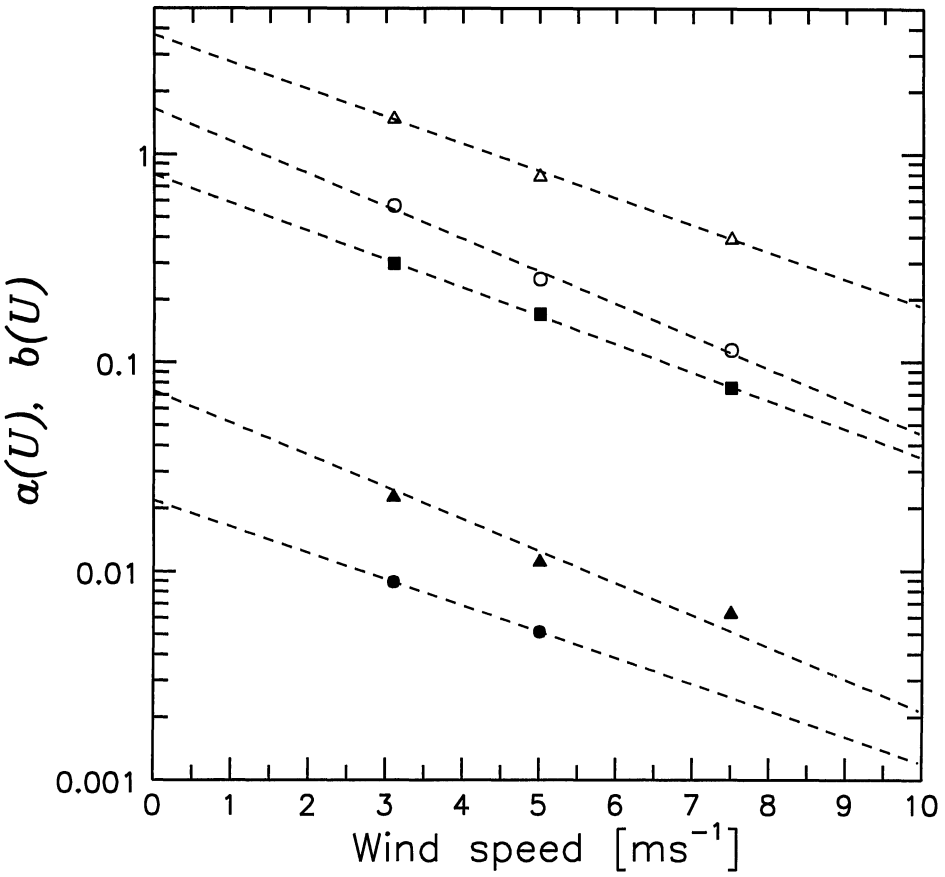

Figure 13. Amplitude $a(U)$ (triangles) and bias $b(U)$ (circles) of the wind-speed-dependent modulations of sonic speed ratios (solid) and wind vector deflection (open) plotted against wind speed. Also shown is the change of mean tilt with wind speed (squares). The dashed lines are exponential functions fitted to the data points. The corrections increase with decreasing wind speed and may reach almost 10%, 5°, and 0.8°, respectively, at very low wind speeds.

Stability of calibration

A point of major interest with respect to the deployment of sonic anemometers for prolonged periods of unattended operation is the long-term stability of calibration. Investigations by Kraan and Oost (1989), in which a Kaijo Denki sonic anemometer (DAT-300/TR-61A) was calibrated in a wind tunnel several times during a four year period, indicate that the horizontal response may change as much as 10% over periods as short as 6 months. Such large changes were not experienced during the present investigation. Fig. 14 shows the results of two consecutive calibration runs with the same sonic anemometer and under the same experimental conditions. The two runs are separated in time by approx. three years, and it is evident that the wind speed calibration for all practical purposes has remained the same during this period. In addition, the sonic wind speeds were compared to cup anemometer derived wind speeds on a regular basis during the period between the two calibration runs. These comparisons showed only small (random) changes in the ratio of cup to sonic anemometer wind speeds, on the order of 1%.

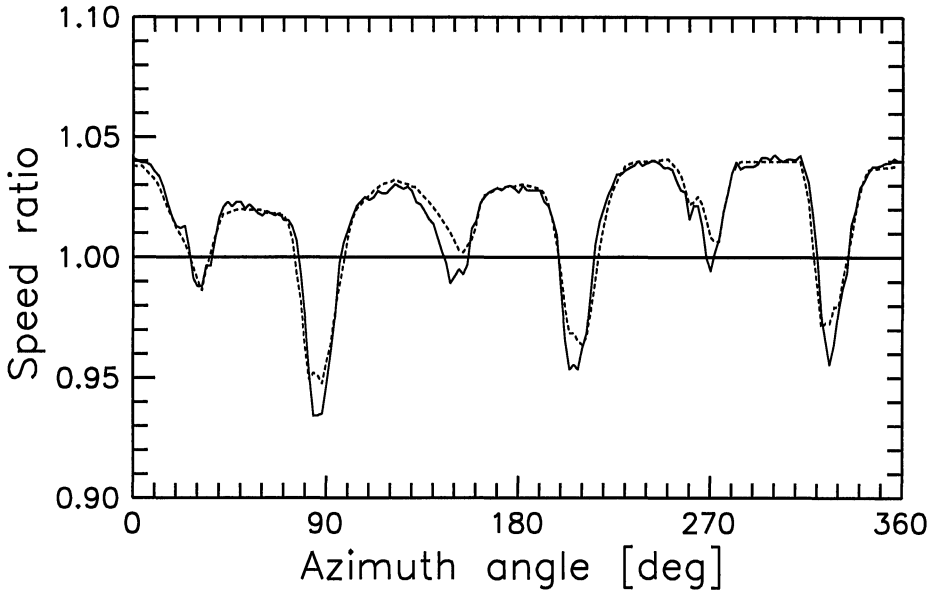

Figure 14. Change in sonic wind speed calibration over a three year period. The full line corresponds to Fig. 7a, the dashed line represents measurements taken in the same wind tunnel three years before. The resolution in azimuth for this run is 2°.

3.2 Non-horizontal flow

The sonic response to an inclined flow (non-horizontal wind vector) was investigated for both different flow directions and flow speeds by tilting the probe head in the tunnel. The true (tunnel) vertical wind speed w_t was obtained from the horizontal flow speed U_t and the angle of inclination of the probe head α: $w_t = U_t \sin\alpha$. The corresponding vertical wind speed from the sonic w_s was calculated from the measured vertical wind speed w_m corrected for the probe-induced tilting of the wind vector $\boldsymbol{U}$: $w_s = w_m - U \sin\alpha_s$. A comparison between sonic-derived vertical wind speeds and vertical wind speeds obtained from the tunnel is shown in Fig. 15 for three characteristic azimuth angles as well as for all measurements, regardless of wind direction. While the overall comparison of sonic and tunnel vertical speeds is quite good (albeit with some scatter), Fig. 15 also shows that the vertical response characteristics of the sonic change significantly with the horizontal angle of attack of the flow. Table 1 lists the slope and intercept of the least-squares-fit lines shown in Fig. 15.

Table 1. Slope and intercept of the least-squares-fit lines shown in Fig. 15.

	$w < 0$		$w > 0$		All w	
Azimuth	Slope	Intercept	Slope	Intercept	Slope	Intercept
240	—	—	—	—	0.844	−0.000
270	1.040	0.018	1.113	−0.037	1.039	0.009
300	0.787	0.004	0.890	0.010	0.843	0.033
330	1.018	0.025	0.994	0.049	1.023	0.031

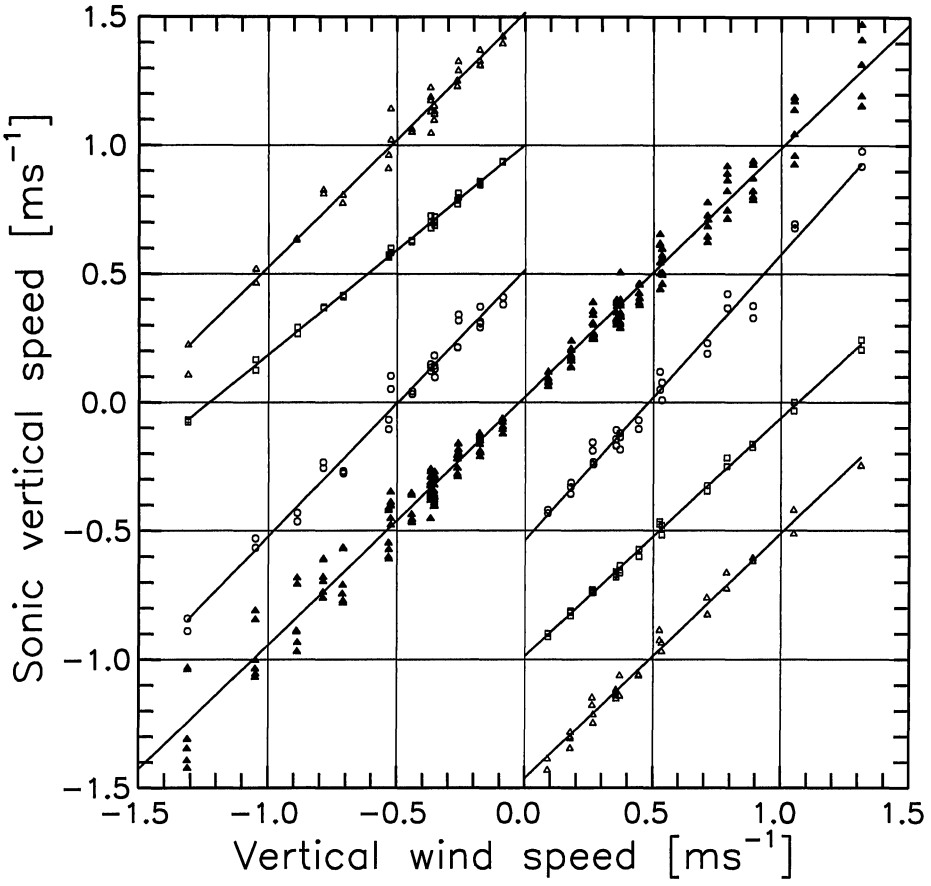

Figure 15. Sonic-derived versus true vertical wind speeds in a wind tunnel. The range of vertical wind speeds shown was obtained with horizontal flow speeds of 3 to 15 ms^{-1} by tilting the sonic probe head through the range from +5° to −5° in the vertical. The overall comparison between w_s and w_t is shown with solid triangles. Sonic speeds have been shifted ±0.5, ±1.0 *and* ±1.5 *ms^{-1} for the comparisons at azimuth angles of* 270° *(circles),* 300° *(squares) and* 330° *(triangles), respectively.*

The sonic-derived wind vector is distorted most when the flow is in the direction of the sound paths (240° and 300°); here the sonic-derived vertical speeds are suppressed by approximately 15%. The scatter of the measurements, however, is less for these directions than for 270° and 330°. The flow is least tilted for flow past the supporting struts (330°) where the mean vertical speeds agree well. For flow between the sound paths (270°) the sonic overestimates the vertical wind speed slightly. Considering the three-dimensional geometry of the probe head, the angular response is relatively complicated. The overall effect of the wind-vector tilting originating in the sonic probe head is found to be a reduction of the vertical wind speed component on the order of 10% for negative and a few per cent for positive vertical speeds.

The vertical response is further illustrated in Fig. 16 where ratios of sonic- to tunnel-derived vertical wind speeds are plotted against azimuth - for all azimuths and irrespective of nominal tunnel flow speed. Also shown are the mean ratios and standard deviations of the measurements corresponding to each characteristic azimuth angle. The description given above is confirmed: for flow in the direction of the sound paths ($0° + n \cdot 60°$; $n = 0, 1, \ldots, 5$) the sonic vertical wind speed is about 15% too low; for flow between the sound

paths ($30° + n \cdot 60°$; $n = 0, 1, \ldots, 5$) the sonic vertical speed is close to or slightly higher than the tunnel-derived vertical speed. This suggests that the vertical response can be modeled in a simple and approximate way using a sine function.

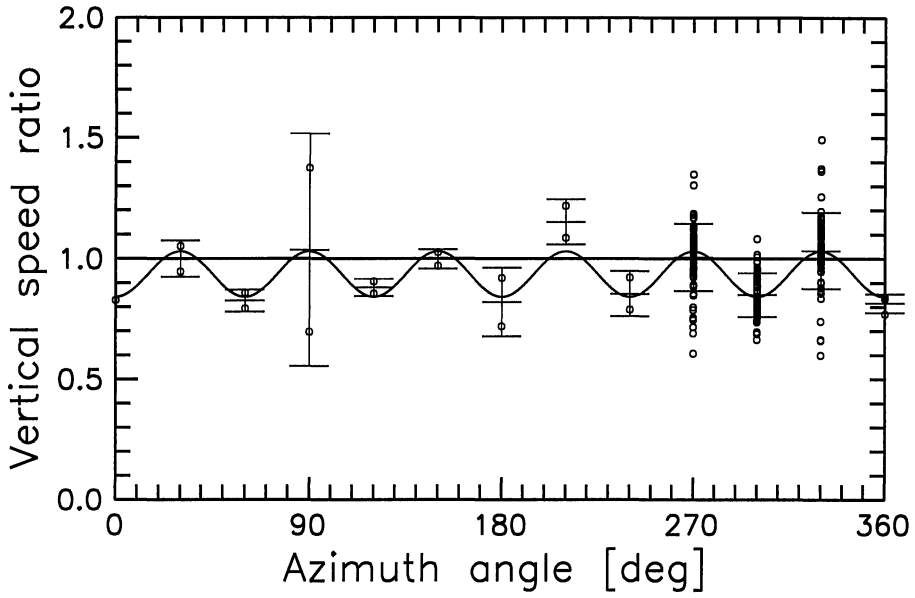

Figure 16. Ratio of sonic-derived to true vertical wind speeds versus azimuth. Mean ratios and standard deviations for each characteristic azimuth are shown by horizontal bars. The full line shows a simple sinusoidal fit to the data.

The scatter among single speed ratios in Fig. 16 is comparable to or greater than the variation in the mean ratios - and is obviously not explained solely by differences in the horizontal angle of attack. Therefore, in Fig. 17 the same ratios of vertical speed have been plotted against the tilt angle of the probe base.

Two sources of scatter are readily identified: first, the scatter increases with numerically decreasing tilt angles. This is to be expected since decreasing tilt angles corresponds to decreasing vertical wind speeds, thus making the (random) errors in the speed ratios relatively larger. Secondly, as illustrated most clearly by the speed ratios obtained at a tunnel speed of 15 ms^{-1}, the ratios show a systematic variation with tilt angle, ie for negative tilt angles (negative w) the ratios decrease with numerically decreasing tilt angles, and for positive tilt angles (positive w) the ratios increase with numerically decreasing tilt angles. This systematic variation corresponds to an offset in the probe base alignment of about $\frac{1}{4}°$.

This possible error in the probe base alignment is investigated further in Fig. 18, where the sonic-derived tilt of the wind vector at a flow speed of 10 ms^{-1} and a probe base tilt of 0° is shown as a function of the run number ('time') for three different azimuth angles. The figure indicates that the probe base alignment has indeed changed slightly during the three day calibration period; by an amount comparable to $\frac{1}{4}°$.

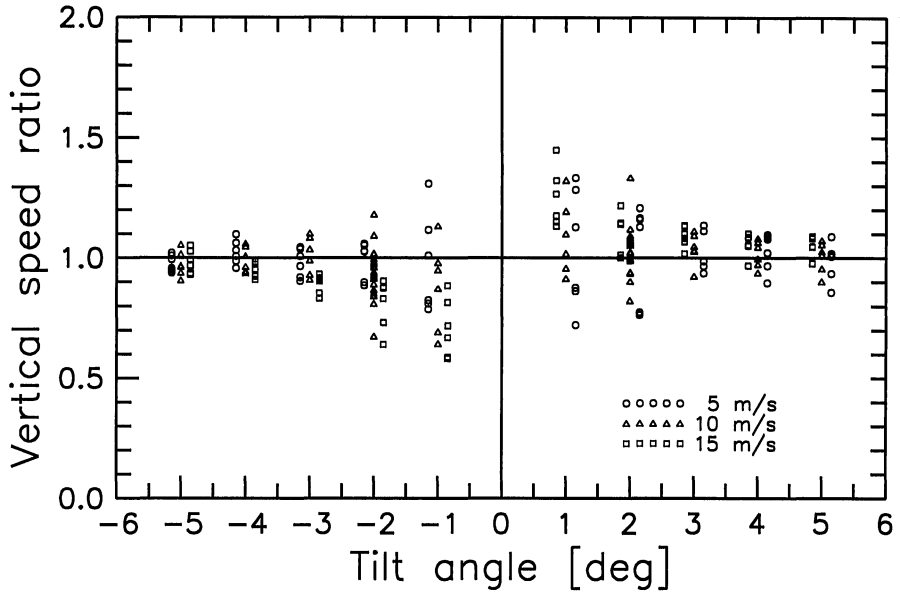

Figure 17. Ratios of sonic-derived to true vertical wind speeds versus tilt angle of the sonic probe base. For the sake of legibility the measurements at tunnel speeds of 5 and 15 ms^{-1} have been offset ±0.2° in tilt angle.

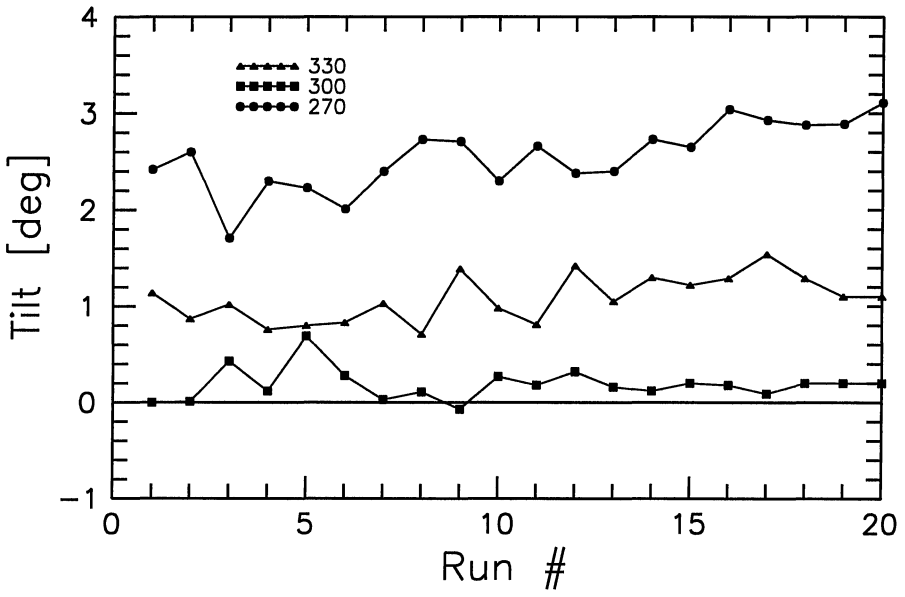

Figure 18. Sonic-derived tilt of the wind vector at a flow speed of 10 ms^{-1} and a probe base tilt of 0° for three different azimuth angles. The tilt is shown as a function of the run number ('time').

4 Preliminary field results

The sonic anemometer system was employed from February 1983 to February 1985 in the JYLEX field experiment in western Jutland, Denmark. The sonic probe was mounted at a height of 5.5 m on a 24-meter meteorological mast. Further, the mast contained fast-responding cup-anemometers at heights of 3.0, 9.9 and 23.8 m, wind vanes at 9.9 and 23.8 m, and pt-500 temperature sensors at 2.0 and 22.9 m. The temperature sensors gave the absolute temperature as well as the temperature difference between the two levels. The mean relative humidity (at screen height) and short-wave incoming radiation were measured for prolonged periods.

The mast was in successful operation for about two years. In this period the sonic anemometer system operated continuously for about 85% of the time. The alignment procedure described in Section 2.4, as well as the wind-tunnel-derived calibration curves shown in Fig. 7 (a, b, c), were coded into the data acquisition system and provided real-time calculations of the turbulent energies ($\overline{u'u'}, \overline{v'v'}, \overline{w'w'}$), shear stresses ($\overline{u'w'}, \overline{v'w'}$), and a sound-virtual temperature-based heat flux ($\overline{w'T_s'}$). Also, consecutive 20-min averages of mean wind speed and direction, wind-vector tilt, and air temperature were obtained. The sampling rate was 1 Hz. The profile instrumentation had a corresponding efficiency of more than 95%. The basic data set thus consists of more than 40 000 20-min values from each sensor.

The mast was situated in an agricultural area, mainly with corn fields. The area is extremely flat and devoid of buildings and vegetation other than the crops. The results presented below were obtained in a 135°-sector around SW where the surface is rather horizontal and homogeneous.

4.1 Results from the sonic anemometer

Figure 19 (a,b) shows the ratio of standard deviation of the vertical wind velocity fluctuations and the friction velocity as a function of surface layer stability in terms of z/L, where z is the height (5.5 m) and L is the Monin-Obukhov length. The measurements are shown as mean values of σ_w/u_* in logarithmically equidistant classes of z/L, and the standard deviation in each class is indicated by bars. The data are compared with relations suggested by Merry and Panofsky (1976) and Panofsky and Dutton (1984).

In the unstable regime the measurements agree rather well with both relations though the data points are shifted slightly towards lower values of σ_w/u_*. On the stable side (Fig. 19b) σ_w/u_* is seen to be more or less constant to a z/L of about 1-2 ($L \approx 3-5$ m), as suggested by Panofsky and Dutton (1984). For very stable conditions the scatter increases, but the data indicate an increasing ratio.

The ratios σ_u/u_*, σ_v/u_* and σ_w/u_* for near neutral stability were found to be 2.56, 1.83, and 1.15, respectively. These values are within 10% of the average values given in Panofsky and Dutton (1984, Table 7.1): 2.39, 1.92, and 1.25.

4.2 Results from sonic and profile instrumentation

Figure 20 compares the 20-min averaged wind speed at 5.5 m, measured by the sonic anemometer, with the corresponding wind speed derived from the profile instrumentation.

The agreement between sonic- and profile-derived wind speeds is seen to

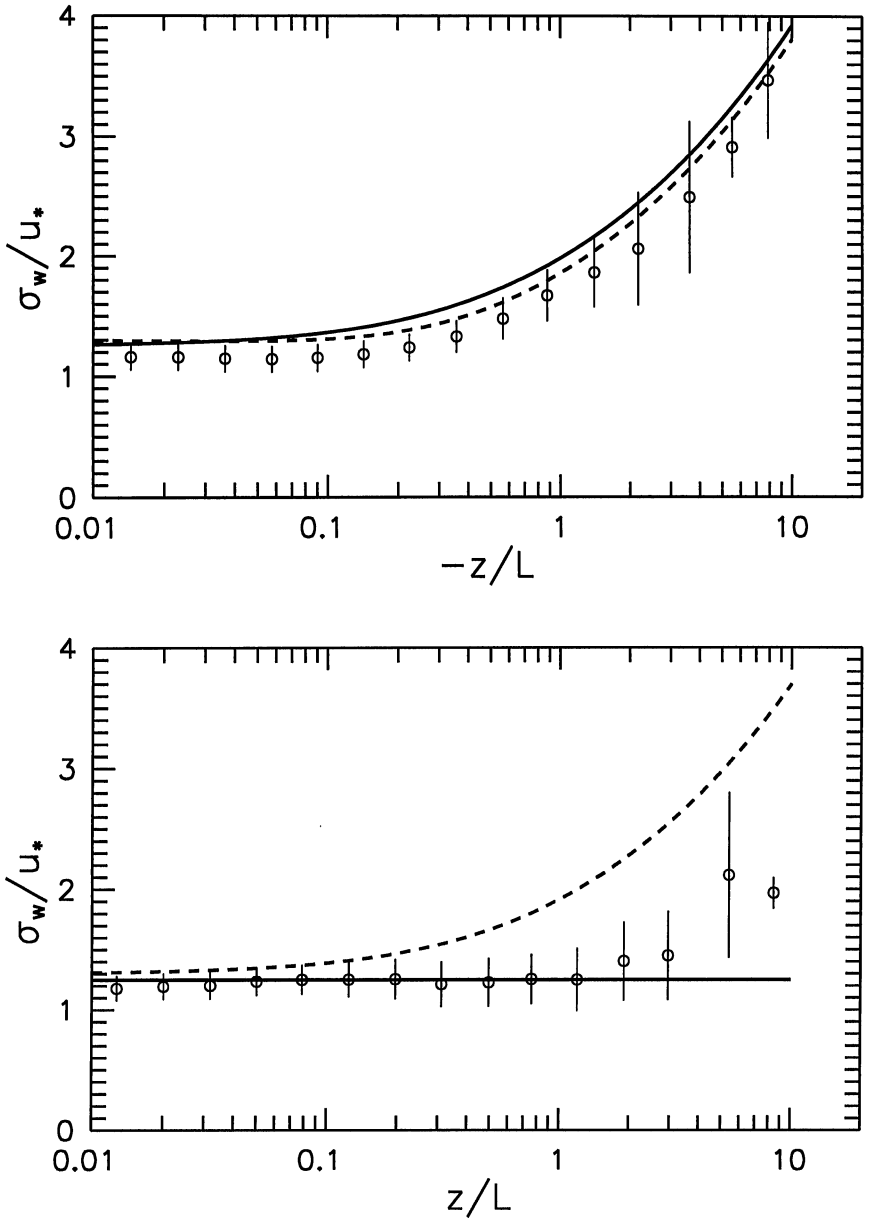

Figure 19. σ_w/u_* as function of z/L for unstable (a) and stable (b) conditions. The curves are from Merry & Panofsky (1976) (dashed) and Panofsky & Dutton (1984) (full line).

be excellent. Furthermore, the ratio of profile and sonic wind speeds has been analyzed as a function of time, wind direction, wind speed and stability. These investigations showed that i) no drift in calibration of the sonic system could be discerned during 19 months of operation, ii) the correction of the sonic horizontal wind speeds (Fig. 7 a) effectively removes any variation with wind direction of the ratio $U_{\text{cup}}/U_{\text{sonic}}$, iii) the mean overspeeding correction of the cup anemometers amounts to about 1% and, when applied, makes the ratio practically invariant with wind speed and stability.

As an example of the application of the sonic anemometer system, we will finally present a climatological investigation of the flux-profile relationship for momentum. The dimensionless gradient of wind speed in the surface layer,

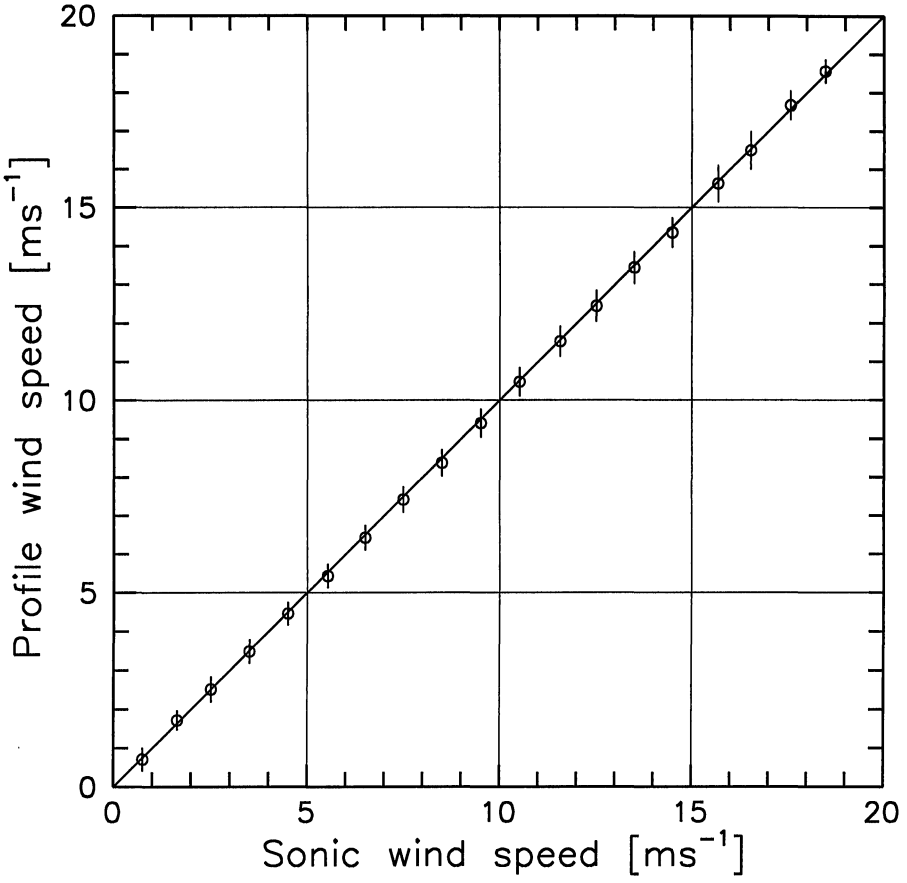

Figure 20. Profile-derived versus sonic wind speeds at 5.5 m a.g.l. Standard deviation of each 1 ms^{-1}-class indicated.

Φ_m, is by definition given as

$$\Phi_m = k\frac{z}{u_*}\frac{\partial \overline{u}}{\partial z} \tag{41}$$

where k is the von Kármán constant, u_* is the friction velocity and $\partial\overline{u}/\partial z$ is the gradient of mean wind speed at height z. $\partial\overline{u}/\partial z$ was found by differentiating mathematical expressions fitted to the wind speed profile. The friction velocity is obtained directly from the sonic anemometer as $\sqrt[4]{\langle u'w'\rangle^2 + \langle v'w'\rangle^2}$. Prescribing a value of unity for $\Phi_m(0)$ at neutral conditions leads to a von Kármán constant of 0.375, which is used in the following. Figure 21 shows the dimensionless wind speed gradient as a function of atmospheric stability in terms of the gradient Richardson number.

Again, the number of observations allows us to present the data in logarithmically equidistant classes of stability. The standard deviation in each class is given by bars. The Richardson number was chosen as scaling parameter because it turned out to be a better statistic for describing $\Phi_m(0)$ in the unstable regime (Mortensen, 1985). Also shown is a Businger-Dyer-like representation of $\Phi_m(0)$ for unstable conditions

$$\Phi_m(Ri) = (1 - a \cdot Ri)^n \qquad Ri < 0 \tag{42}$$

In our case the value of 12 for a and an exponent of $-1/3$ yield good agreement with the measurements. The result of a similar analysis in the stable regime is shown in Fig. 22.

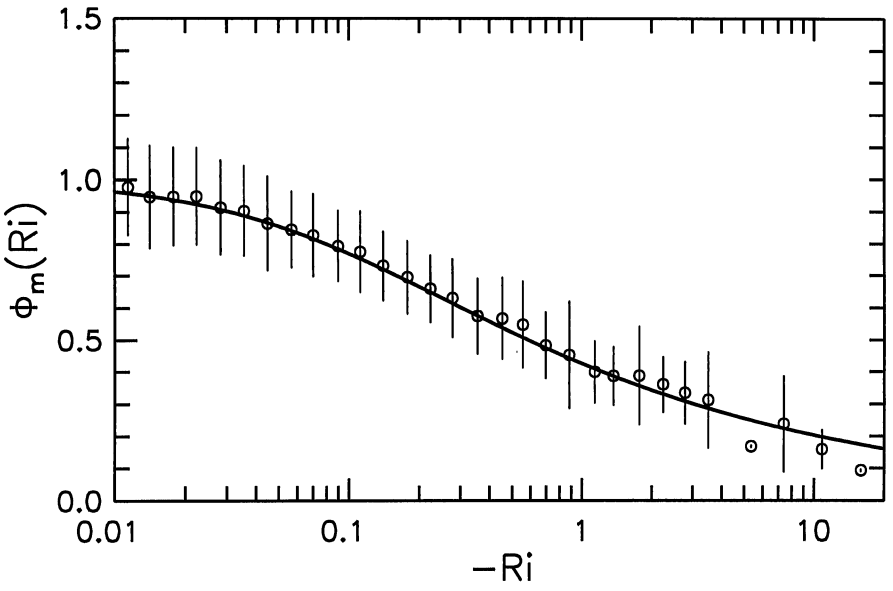

Figure 21. The dimensionless gradient of wind speed as a function of gradient Richardson number for unstable conditions.

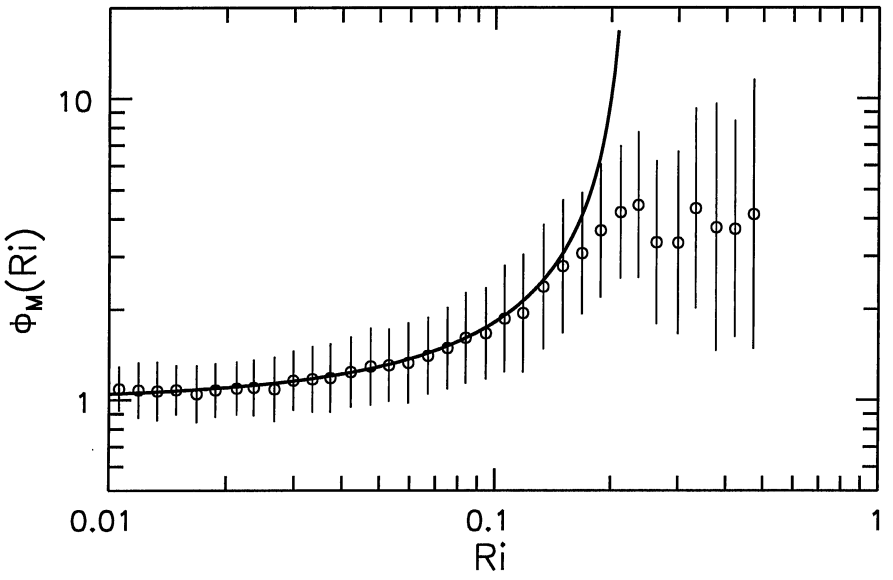

Figure 22. As Fig. 21, but for stable conditions.

For Richardson numbers less than 0.15 the measurements are described well by a relation of the form:

$$\Phi_m(Ri) = (1 - b \cdot Ri)^{-1} \qquad 0 < Ri < 0.15 \tag{43}$$

A value of 4.5 was used for b in Fig. 22.

5 Summary and conclusions

The described sonic anemometer and data acquisition system have proven a very sturdy and reliable turbulence instrument for unattended operation over prolonged periods. This is true for the above-mentioned field experiment and also for several air-sea interaction, diffusion and wind engineering studies, in which the system has been employed under a wide range of meteorological conditions.

Based on an analysis of the geometry of the probe head and a comprehensive wind tunnel investigation of the sonic response, the following conclusions may be drawn:

- The flow around the TR-61B probe head is significantly distorted and the instrument must be carefully calibrated in order to obtain accurate measurements of the wind components. This is firmly supported by field comparisons with eg cup anemometers.
- The geometry of the transducer setup as well as the lengths of the three sound paths are found to conform closely to the design specifications. The errors introduced by the built-in transformation of the wind components are therefore negligible.
- The horizontal response varies by more than 15% as a function of both wind direction (angle of attack) and speed. The flow distortion originating in the probe head structure itself seems to be invariant with flow speed, but depends strongly on the geometry of the probe head. A cyclic, flow-speed-dependent part of the distortion can be attributed mainly to the specific mounting of the signal cables below the probe base.
- Expressions have been derived to assess the transducer shadow effects for the TR-61B probe, but these cannot explain the response of the sonic.
- The directional response varies by more than 5° as a function of both azimuth and flow speed. The deflection of the flow vector can also be described as a combination of a speed-independent part, reflecting the geometry of the sensor, superimposed with a cyclic, speed-dependent part, reflecting the signal cables.
- The flow vector is tilted upwards between 0 and 3° depending on azimuth angle, but shows little variation with flow speed. The mean tilt increases slightly with decreasing speed, but apparently not in a cyclical manner. Consequently, the signal cables and their attachment seem to have no influence on the tilt - a somewhat surprising observation.
- Based on two calibration experiments within three years, as well as systematic field comparisons with cup anemometers, it is concluded that the (horizontal) response of the sonic system has remained essentially constant over this period of time.
- Even after correction for the probe-induced tilting of the flow vector, the effect of the probe head on the vertical response is a marked reduction in the measured vertical speed component, on the order of 10%.
- Calibration functions and an ad-hoc calibration procedure are finally proposed. The means and sample standard deviations of the horizontal speed ratio, the direction difference and the vertical speed ratio after the calibration procedure has been applied are 1.00 ± 0.01, $0.08° \pm 0.29°$ and 1.00 ± 0.13, respectively.

- Expressions for calculating the sound-virtual temperature from the transit times, taking into account the translation of the sound wave field due to the flow speed component perpendicular to the sound path, have been derived. An exact correction term to the DAT-300 temperature output follows directly.

The greatest uncertainty in the turbulence statistics obtained with the sonic system seems to be associated with the vertical angular response of the sensor, ie the suppression of the vertical wind velocity component. Further investigations will be conducted to resolve this difficulty in more detail. The generally good agreement between the observations and previously established relationships is encouraging to this continued effort.

Finally, it should be noted that the wind-speed-dependent part of the flow distortion, originating in the signal cables below the probe base, is probably characteristic of this probe design only. Minor design changes or changes in the specific mounting of the cables will most likely change the characteristics and/or magnitude of this part of the distortion.

Acknowledgements

The wind tunnel calibrations, as well as the JYLEX field experiment, were initiated and implemented by S.E. Larsen and I. Troen of the Meteorology Section at Risø. G. Jensen, also of the Meteorology Section, carried out most of the wind tunnel measurements.

The guidance and inspiration offered by S.E. Larsen during the course of this work is gratefully acknowledged. Further, the author wishes to thank G. Geernaert, Naval Research Laboratory, for many valuable comments on an early draft of this report.

The report was finished while the author was as a visiting scientist at the National Center for Atmospheric Research, Boulder, CO. Thanks are due to W.F. Dabberdt, T. Horst and S. Oncley of the Atmospheric Technology Division.

References

Hanafusa, T., T. Fujitani, Y. Kobori and Y. Mitsuta (1982). A new type sonic anemometer-thermometer for field operation. *Papers in Meteorology and Geophysics* **33**, 1-19.

Kaijo Denki (1982). Digitized ultrasonic anemometer-thermometer model DAT-300. Instruction manual. Kaijo Denki Co. Ltd., Tokyo, 62 p.

Kaimal, J.C. (1979). Sonic anemometer measurement of atmospheric turbulence. *Proc. Dynamic Flow Conference*, Skovlunde, Denmark (DISA Electronic A/S), 551-565.

Kaimal, J.C. and J.E. Gaynor (1991). Another look at sonic thermometry. *Boundary-Layer Meteorol.* **56**, 401-410.

Kelley, N.D., G.N. Scott and J.S. Allread (1990). A discussion of the results of an in-situ comparison of three, full-vector anemometers. *Seventh Symposium on Meteorological Observations and Instrumentation*, New Orleans, January 14-18, 1991, 80-85.

Kraan, C. and W.A. Oost (1989). A new way of anemometer calibration and its application to a sonic anemometer. *J. Atmos. Ocean. Tech.* **6**, 516-524.

Merry, M. and H.A. Panofsky (1976). Statistics of vertical motion over land and water. *Quart. J. Roy. Meteor. Soc.* **102**, 255-260.

Mortensen, N.G. (1985). Dimensionless gradients of wind speed and temperature in the atmospheric surface layer (Dimensionsløse gradienter af vindhastighed og temperatur i det atmosfæriske overfladelag). In Danish. Risø-I-209, 140 p.

Mortensen, N.G., S.E. Larsen, I. Troen and T. Mikkelsen (1986). Two-years-worth of turbulence data recorded by a sonic-anemometer-based data acquisition system. *Sixth Symposium on Meteorological Observations and Instrumentation*, New Orleans, January 12-16, 1987, 393-396.

Panofsky, M.A. and J.A. Dutton (1984). *Atmospheric turbulence.* John Wiley & Sons, New York. 397 p.

Wyngaard, J.C. and S.-F. Zhang (1985). Transducer-shadow effects on turbulence spectra measured by sonic anemometers. *J. Atmos. Ocean. Tech.* **2**, 548-558.

Zhang, S.-F., J.C. Wyngaard, J.A. Businger and S.P. Oncley (1986). Response characteristics of the U.W. sonic anemometer. *J. Atmos. Ocean. Tech.* **3**, 315-323.

A Correction of sonic-measured winds

The Kaijo Denki sonic anemometer provides measurements of the wind vector components u_s, v_s, and w_s, in a three-dimensional fixed Cartesian coordinate system, the x-axis of which points in the easterly, the y-axis in the northerly, and the z-axis in the vertical direction. To correct for sonic internal flow distortion the ad-hoc calibration procedure described below may be applied.

The sonic-measured wind direction Θ_s and horizontal wind speed U_s are determined from u_s and v_s:

$$\Theta_s = \arctan_2(-u_s, -v_s) \tag{A.1}$$

$$U_s = \sqrt{u_s^2 + v_s^2} \tag{A.2}$$

The true wind direction Θ_t is determined from the sonic wind direction Θ_s in two steps. First, a preliminary wind direction Θ_p is obtained by inverting the correction table depicted in Fig. 7 c:

$$\Theta_p = \Theta_s - G(10, \Theta_s) \tag{A.3}$$

where $G(10, \Theta)$ is the wind vector deflection measured in the wind tunnel at 10 ms^{-1}. Secondly, the wind speed dependency is taken into account:

$$\Theta = \Theta_p - g(10, \Theta_p) + g(U_s, \Theta_p) \tag{A.4}$$

Here, $g(U, \Theta)$ is of the form $a(U)\cos(\Theta + \phi) + b(U)$. The angle ϕ may be quite sensitive to the specific mounting of the cables; a value of 30° is used here. The amplitude and bias of the flow speed dependent modulations are of the form $Ae^{B \cdot u}$.

A preliminary horizontal wind speed U_p is determined from the sonic wind speed U_s by applying the correction table depicted in Fig. 7 a:

$$U_p = \frac{U_s}{F(10, \Theta)} \tag{A.5}$$

where $F(10, \Theta)$ is the azimuth-dependent speed ratio measured in the wind tunnel at 10 ms^{-1}.

The total correction factor $F(U, \Theta)$, which depends on both azimuth and wind speed, can now be determined from U_p and Θ:

$$F(U_p, \Theta) = F(10, \Theta) + a(U_p)\sin(\Theta - 15) + b(U_p) \tag{A.6}$$

Also in this case are the amplitude and bias of the flow speed dependent modulations of the form $Ae^{B \cdot u}$.

The horizontal wind speed U can now be determined from the sonic horizontal wind speed U_s by use of the total correction factor:

$$U = \frac{U_s}{F(U_p, \Theta)} \tag{A.7}$$

Finally, the components u and v of the corrected horizontal wind speed U can be determined from:

$$u = -\sin\Theta \cdot U \tag{A.8}$$

$$v = -\cos\Theta \cdot U \tag{A.9}$$

Having corrected for the horizontal response of the sonic probe the length of the wind vector V can now be approximated by

$$V = \sqrt{U^2 + w_s^2} \tag{A.10}$$

The measured tilt of the wind vector is

$$\alpha_s = \arctan\left(w_s/\sqrt{u_s^2 + v_s^2}\right) \tag{A.11}$$

To correct for the probe-induced tilt of the wind vector we apply the table depicted in Fig. 7 b

$$\alpha_p = \alpha_s - [H(10,\Theta) + h(U)] \tag{A.12}$$

where $H(10,\Theta)$ is the azimuth-dependent wind vector tilt measured in the wind tunnel at 10 ms^{-1} and $h(U)$ is a correction for the change in mean tilt as a function of wind speed ($h(U) = Ae^{B\cdot U}$). The vertical speed is now

$$w_p = V \cdot \sin\alpha_p \tag{A.13}$$

Finally, the periodic suppression of the vertical component for flow in directions of the sound paths is taken into account

$$\frac{w_p}{w} = A\sin(\Theta + \phi) + B \tag{A.14}$$

The amplitude and bias of the flow-speed dependent modulations of the speed ratio (A.6), deflection (A.4), and mean tilt (A.12) are given in Tab. 2.

Table 2. Amplitude $a(U)$ and bias $b(U)$ of the wind-speed-dependent modulations of sonic speed ratio and wind vector deflection, cf. Fig. 15. Also listed is the change of mean tilt with wind speed.

	Amplitude $a(U)$	Bias $b(U)$	ϕ
Speed ratio	$0.073\exp(-0.3545\cdot U)$	$0.028\exp(-0.3545\cdot U)$	15°
Deflection	$3.737\exp(-0.3017\cdot U)$	$1.654\exp(-0.3614\cdot U)$	30°
Mean tilt	—	$0.798\exp(-0.3141\cdot U)$	—

Bibliographic Data Sheet **Risø-R-704(EN)**

Title and author(s)

Flow-response characteristics of the Kaijo Denki omni-directional sonic anemometer (TR-61B)

Niels G. Mortensen

ISBN	ISSN
87-550-1921-8	0106-2840

Dept. or group	Date
Meteorology and Wind Energy	April 1994

Groups own reg. number(s)	Project/contract No.
AMV 01009-05	-

Pages	Tables	Illustrations	References
31	2	22	12

Abstract (Max. 2000 char.)

This report describes a commercially available, three-dimensional sonic anemometer/thermometer: the Kaijo Denki DAT-300 fitted with an omni-directional sensor, the TR-61B probe head. Based on an analysis of the probe geometry and a comprehensive wind tunnel investigation it is found that the flow around the probe head is significantly distorted. Sonic-derived horizontal wind speed, wind direction and wind vector tilt deviate by as much as 15%, 5° and 3°, respectively, from the corresponding quantities in the wind tunnel. The flow distortion reflects strongly the geometry of the probe head and is partly dependent on the flow speed. Expressions are derived to assess the transducer shadow effect, but these alone cannot explain the response characteristics of the sonic. Instead, an ad-hoc calibration procedure is suggested, employing correction tables based on the wind tunnel measurements. The corrected horizontal and vertical wind speed components compare well to the wind tunnel, even though the vertical response shows some scatter. Preliminary field investigations support the correction scheme and suggest that the calibration may be stable over periods of several years.

Expressions for calculating the sound-virtual temperature from the transit times, taking into account the translation of the sound wave field due to the flow speed component perpendicular to the sound path, have been derived. An exact correction term to the sonic temperature output follows directly.

Descriptors INIS/EDB

ACOUSTIC MEASUREMENTS; ANEMOMETERS; CALIBRATION; SHADOW EFFECT; SONIC PROBES; TEMPERATURE MEASUREMENT; TURBULENCE; VELOCITY; WIND

Available on request from:
Risø Library, Risø National Laboratory (Risø Bibliotek, Forskningscenter Risø)
P.O. Box 49, DK-4000 Roskilde, Denmark
Phone (+45) 46 77 46 77, ext. 4004/4005 · Telex 43 116 · Fax (+45) 46 75 56 27

RISØ

OBJECTIVE

The objective of Risø National Laboratory is to further technological development in three main areas: energy, environment and materials.

USERS

Risø's scientific results are widely applied in industry, agriculture and public services. Risø contributes its share of new knowledge to the global research community.

RESEARCH PROFILE

Risø emphasises long-term and strategic research providing a solid scientific foundation for the technological development of society.

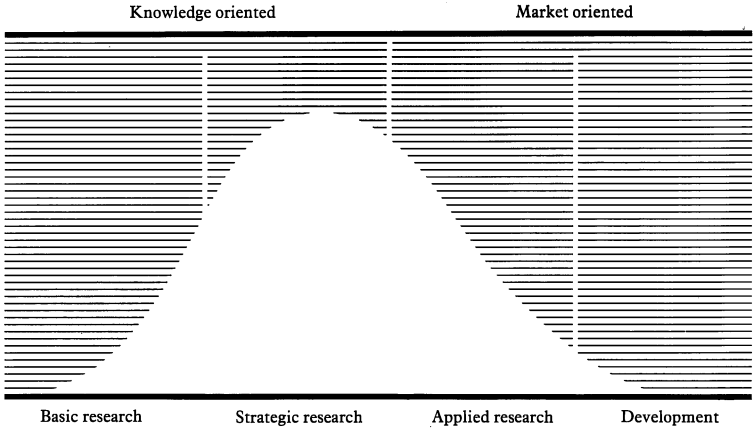

PRIORITY AREAS

* **Combustion and gasification**
* **Wind energy**
* **Energy materials**
* **Energy and environmental planning**
* **Assessment of environmental loads**
* **Reduction of environmental loads**
* **Safety and reliability of technical systems**
* **Nuclear safety**
* **Atomic structure and properties of materials**
* **Advanced materials and materials technologies**
* **Optics and fluid dynamics**

Risø-R-704(EN)
ISBN 87-550-1921-8
ISSN 0106-2840

Available on request from:
Risø Library
Risø National Laboratory
P.O. Box 49, DK-4000 Roskilde, Denmark
Phone +45 46 77 46 77, ext. 4004/4005
Telex 43116, Telefax 46 75 56 27